Role of Cyclic Ether and Solvent in a Non-Alkoxide Sol−Gel Synthesis of Yttria-Stabilized Zirconia Nanoparticles

Christopher N. Chervin,[†,‡] Brady J. Clapsaddle,[§] Hsiang Wei Chiu,[†] Alexander E. Gash,[§] Joe H. Satcher, Jr.,[§] and Susan M. Kauzlarich*[,†]

Department of Chemistry, University of California at Davis, One Shields Avenue, Davis, California 95616, University Outreach and Chemistry and Materials Science Directorate, Lawrence Livermore National Laboratory, Livermore, California 94550

Received May 30, 2006. Revised Manuscript Received July 13, 2006

The effects of cyclic ether (epoxide versus oxetane), solvent, and drying method were examined for a non-alkoxide sol−gel synthesis of yttria-stabilized zirconia (YSZ). YSZ sol−gel materials, from 3 to 25 mol % Y_2O_3, were successfully prepared with either propylene oxide (PO) or trimethylene oxide (TMO) in both aqueous and mixed ethanol−water solutions of Zr^{4+} and Y^{3+} chlorides. Supercritical drying (aerogels) produced fine, nanoparticulate networks, whereas drying under ambient conditions (xerogels) resulted in heterogeneous micrometer-sized hard agglomerates. The resulting materials were characterized using powder X-ray diffraction (XRD), Raman spectroscopy, transmission electron microscopy, scanning electron microscopy, nitrogen adsorption/desorption analysis, and elemental analysis by inductively coupled plasma−atomic emission spectroscopy. The cyclic ether and solvent were found to be critical factors in the resulting as-prepared aerogel surface area and morphology. For a given solvent, aerogels prepared with PO had higher surface areas than did those prepared with TMO. For example, the surface areas of aerogels prepared in water were 453 and 295 m^2/g for PO and TMO, respectively. Following calcination to 550 °C, however, the crystallized YSZ powders were similar, consisting of homogeneous nanoparticles (∼10 nm) with spherical morphologies and high surface areas (>100 m^2/g). Elemental analysis, XRD, and electron microscopy indicated that Y_2O_3 and ZrO_2 formed a homogeneous nanostructure over a wide range of Zr/Y ratios, corresponding to 3−25 mol % Y_2O_3.

Introduction

Yttria-stabilized zirconia (YSZ), a high-temperature oxide conductor, is a technologically significant material that finds extensive use as a solid-state electrolyte in applications such as solid oxide fuel cells and oxygen sensors.[1] Recently, we reported the aerogel synthesis of homogeneous, nanoparticulate 9 mol % YSZ using an epoxide-initiated sol−gel method.[2] The amorphous aerogel crystallized into YSZ below 550 °C, producing a homogeneous powder with a high surface area (159 m^2/g) and spherical particles with diameters of ∼10 nm. In that work, YSZ was synthesized by the addition of propylene oxide to aqueous solutions of Zr^{4+} and Y^{3+} chlorides.[2] In this study, we investigated the effects the cyclic ether (epoxide (oxirane) versus a four-membered ring ether (oxetane)), solvent, and drying method have on surface area, morphology, and crystallization of the resultant YSZ. The inclusion of Y_2O_3 into the ZrO_2 structure over a wide range of Zr/Y ratios, corresponding to 3−25 mol % Y_2O_3, was also studied. Finally, the crystalline products over that substitution range were characterized with powder X-ray diffraction (XRD) and Raman spectroscopy, two complimentary methods for evaluating the change in crystal structure with increasing Y_2O_3 substitution.

In the "epoxide addition method", solutions of hydrated metal salts, assisted by the proton-scavenging properties of an organic cyclic ether, are induced to undergo hydrolysis and condensation reactions to form metal oxide sol−gel materials.[3] The mechanism of proton scavenging is reported to occur in two steps: (1) reversible protonation of the ether ring by hydrolysis of the metal aquocation and (2) nucleophilic attack of the protonated ring by the counterion. As a result, the cyclic ether undergoes irreversible ring opening, which effects a homogeneous rise in the solution pH.[3] The reactivity of the cyclic ether, which is related to the stability of the protonated ring, plays an important role in the kinetics of gelation and resulting morphologies of the wet gels and aerogel products.[4]

The "epoxide addition" method does not require alkoxide precursors, thereby expanding metal oxide sol−gel chemistry to a broad range of elements, including the transition and rare-earth metals. It is a relatively straightforward and versatile technique and can be used to make mono-, binary, and ternary oxides.[5−8] A more complete understanding of

* To whom correspondence should be addressed. E-mail: smkauzlarich@ucdavis.edu. Fax: 530-752-8995. Phone: 530-752-4756.
† University of California at Davis.
‡ University Outreach, Lawrence Livermore National Laboratory.
§ Chemistry and Materials Science Directorate, Lawrence Livermore National Laboratory.

(1) Subbarao, E. C.; Maiti, H. S. *Solid State Ionics* **1984**, *11* (4), 317−338.
(2) Chervin, C. N.; Clapsaddle, B. J.; Chiu, H. W.; Gash, A. E.; Satcher, J. H.; Kauzlarich, S. M. *Chem. Mater.* **2005**, *17* (13), 3345−3351.
(3) Gash, A. E.; Tillotson, T. M.; Satcher, J. H., Jr.; Poco, J. F.; Hrubesh, L. W.; Simpson, R. L. *Chem. Mater.* **2001**, *13* (3), 999−1007.
(4) Gash, A. E.; Satcher, J. H., Jr.; Simpson, R. L. *Chem. Mater.* **2003**, *15* (17), 3268−3275.

10.1021/cm061258c CCC: $33.50
Published on Web 08/31/2006

the effects of the solvent, cyclic ether, and drying method are important for generalizing the epoxide addition method and expanding the benefits of sol−gel chemistry to elements previously inaccessible because of difficulty in preparing or handling their alkoxide precursors.

Experimental Section

Synthesis of YSZ Gels. Yttria-stabilized zirconia (YSZ) precursor sol−gel materials were prepared by the epoxide addition method. The resulting gels were processed by supercritical drying in $CO_2(l)$ (aerogel) or by drying in air at room temperature for 7 days (xerogel). Anhydrous $ZrCl_4$ (99.9+%, Aldrich), $YCl_3 \cdot 6H_2O$ (99.9%, Aldrich), propylene oxide (PO; 99%, Aldrich), trimethylene oxide (TMO; 97%, Aldrich), and absolute ethanol (200 proof, Aaper) were used as received.

The synthesis of 9 mol % YSZ using propylene oxide (PO) in water has been described in detail previously.[2] A similar synthetic method was used in this study. Briefly, stoichiometric amounts of $ZrCl_4$ and $YCl_3 \cdot 6H_2O$ were dissolved in the desired solvent and stirred for 1 h to ensure complete dissolution of the salts. Subsequently, a preweighed amount of epoxide (PO) or oxetane (TMO) was added rapidly with continuous stirring until gelation occurred. Three solvent systems were investigated: (1) distilled water, (2) 1:1 (wt/wt) mixture of ethanol-distilled water (EW (1:1)), and (3) 5:1 (wt/wt) mixture of ethanol-distilled water (EW (5:1)). The effects of cyclic ether and solvent type on gelation rate and resulting aerogel surface area, pore volume, average pore diameter, and powder morphology were studied for a Zr/Y ratio of 5.13 (9 mol % Y_2O_3-stabilized ZrO_2). Additionally, gels with varying Zr/Y ratios were prepared in water using PO addition to investigate the incorporation of Y_2O_3 into ZrO_2.

Following gelation, the gels were aged for 24 h under ambient conditions in closed containers. The aged gels were then washed with ethanol for 3 days, with fresh ethanol exchanged daily. Wet gels were transferred to a Polaron supercritical point drier in which they were processed to aerogels by supercritical drying with CO_2. The pore liquid in the wet gel pores was exchanged for $CO_2(l)$ for 2−3 days, after which the temperature of the vessel was ramped up to ∼45 °C, while a pressure of ∼100 bar was maintained. The vessel was then depressurized at a rate of ∼7 bar/h. Xerogels presented in this study were prepared by drying wet gels in air at room temperature for at least 7 days. Aerogels and xerogels were calcined in air at 550 and 1000 °C by heating at 2 °C /min and holding at the maximum temperature for 1 h, to study the resulting crystal structures and morphologies.

Physical Characterization. Surface area and pore volume and size analyses were performed using an ASAP 2000 surface area analyzer (Micromeritics Instrument Corp.). Prior to analysis, samples of approximately 0.1 to 0.2 g were heated to 200 °C under vacuum (1×10^{-5} Torr) for at least 24 h to remove adsorbed species. Nitrogen adsorption data were taken at five relative pressures from 0.05 to 0.20 at 77 K, and the surface area calculated using BET (Brunauer−Emmett−Teller) theory. Average pore size and pore volumes were calculated from adsorption−desorption data based on the BJH (Barrett−Joyner−Halenda) method using the data points from the desorption branch of the isotherm.

Brightfield transmission electron microscopy (TEM) analyses of aerogels, as-prepared and after calcination at 550 °C, were performed on a Philips CM-12 TEM, operating at 100 keV. TEM samples were prepared by dipping holey carbon-coated 400-mesh grids into methanol colloids of the respective powders, followed by drying at 120 °C overnight. Scanning electron microscopy was performed on aerogel and xerogel samples as-prepared and after calcination at 550 °C using a Philips 30XL FEG SEM operated at 5 keV. SEM samples were prepared by applying drops of methanol colloids of the respective powders onto hot aluminum SEM stubs, followed by drying at 120 °C overnight.

The crystallization temperature of YSZ from an as-prepared aerogel was investigated by in situ temperature-profile XRD using an Inel diffractometer operating at 30 A and 30 keV with Cu Kα radiation. The diffractometer was equipped with a furnace-heated sample holder and a position-sensitive detector, allowing for diffraction measurements at selected temperatures during the calcination process. Diffraction data at the desired temperatures were collected for 30 min. At each temperature, the system was held for an additional hour after the first measurement and a second diffraction pattern was collected. The dwell time and additional XRD scan was to determine if prolonged calcination at low-temperature could induce crystallization. Measurements were made approximately every 100 °C; however, to avoid redundancy, we reported only patterns for selected temperatures. Room-temperature powder XRD patterns of as-prepared and calcined xerogels and aerogels were measured using a Scintag PAD V diffractometer operating at 40 A and 45 keV with Cu Kα radiation. Average crystallite sizes were calculated with the Scherrer formula using the full width at half-maximum (fwhm) of the (111) reflection (100% peak). Calculations were made from whole pattern fitting using a Pearson-VII profile shape function with the Jade 6 powder XRD analysis program (MDI, USA).

Raman spectra of YSZ aerogels prepared with varying Zr/Y ratios and calcined to 1000 °C were obtained to observe the change in crystallographic symmetry with Y_2O_3 addition. For comparison, a Raman spectrum of a commercial 8-mol % YSZ (TZ-8Y, Tosho) powder was measured. The Raman spectra from 100 to 800 cm^{-1} were collected at room temperature for powdered samples using a Jobin Yvon Horiba HR 800 spectrometer. The Raman scattering was excited by a YAG laser source (wavelength of 532.0 nm) at 36 mW.

Elemental analysis of YSZ aerogels with Zr/Y ratios corresponding to 3−25 mol % Y_2O_3 substitution were determined by inductively coupled plasma−atomic emission spectroscopy (ICP−AES) by Galbraith Laboratories of Knoxville, TN, or Desert Analytical Laboratories of Tucson, AZ. The aerogels were calcined to 1000 °C prior to elemental analysis.

Results and Discussion

Synthesis of YSZ Gels. Addition of the epoxide, PO, or the oxetane, TMO, to aqueous or ethanolic aqueous solutions of Zr^{4+} and Y^{3+} chlorides resulted in the formation of white monolithic gels that varied from translucent to opaque depending on the reaction conditions. Table 1 lists the gelation time (t_{gel}) as a function of cyclic ether and solvent for gels prepared with a Zr/Y ratio of 5.13, corresponding to 9 mol % Y_2O_3-stabilized ZrO_2. The t_{gel} times were qualitatively determined as the elapsed time between addition of the cyclic ether and the point at which the sols no longer flowed under the influence of gravity when the reaction containers were tilted.

(5) Clapsaddle, B. J.; Gash, A. E.; Satcher, J. H.; Simpson, R. L. *J. Non-Cryst. Solids* **2003**, *331* (1−3), 190−201.
(6) Clapsaddle, B. J.; Sprehn, D. W.; Gash, A. E.; Satcher, J. H.; Simpson, R. L. *J. Non-Cryst. Solids* **2004**, *350*, 173−181.
(7) Long, J. W.; Logan, M. S.; Carpenter, E. E.; Rolison, D. R. *J. Non-Cryst. Solids* **2004**, *350*, 182−188.
(8) Chervin, C. N.; Clapsaddle, B. J.; Chiu, H. W.; Gash, A. E.; Satcher, J. H., Jr.; Kauzlarich, S. M. *Chem. Mater.* **2006**, *18*, 1928−1937.

Table 1. Summary of YSZ Precursor Gel Times as a Function of Cyclic Ether and Solvent for a Zr/Y Ratio of 5.13[a]

cyclic ether	R_{epox}	R_{H_2O}	t_{gel}
TMO	9	95	5−6 h
TMO	9	EW (1:1)	∼45 min
TMO	9	EW (5:1)	15 s (opaque white)
PO	9	EW (1:1)	25 s (opaque white)
PO	9	EW (5:1)	∼5 s (opaque white)
PO	9	94	75 s
PO	9	150	4.5 min
PO	9	233	22 min
PO	7	94	1.5 min
PO	5	94	4 min

[a] R_{epox} is the molar ratio of cyclic ether to total metals and R_{H_20} is the molar ratio of water to total metals. For the mixed ethanol−water systems (EW (1:1) and (5:1)), R_{H_20} was 95. Unless stated, all gels were monolithic and translucent white.

In general, for a given solvent, the t_{gel} times were significantly shorter for the addition of PO than for TMO. For example, in aqueous solution using similar molar ratios of cyclic ether to total metals (R_{epox}), the t_{gel} times for the addition of PO and TMO were 75 s and 5−6 h, respectively. The shorter t_{gel} times for PO versus TMO addition are consistent with results reported by Gash and co-workers for iron(III) sol−gel materials prepared with the epoxide addition method.[4] PO, an epoxide, contains a three-membered ring, whereas TMO, an oxetane, contains a four-membered ring. Both types of cyclic ethers undergo the same ring-opening reaction; however, the oxetanes undergo these reactions much less readily.[9] Therefore, a slower rise in pH and subsequent longer gelation time are expected for TMO addition. The variation in reaction rate allows some versatility in choosing the appropriate cyclic ether for a given metal salt precursor. It also may provide the opportunity to vary the t_{gel} if desired, such as for casting shaped ceramics or preparing composite materials in which a second phase is suspended in the gel phase.[10]

Gelation occurred more rapidly in ethanol−water solvents than in pure water. The trend in t_{gel} for TMO addition with increasing amount of ethanol was 5−6 h, 45 min, and 15 s for water, EW (1:1), and EW (5:1), respectively. The t_{gel} values for PO addition to similar solutions were 75, 25, and 5 s, respectively. In addition to t_{gel}, solvent and cyclic ether also had an effect on the opacity of the gels. Gels that were prepared with a Zr/Y ratio of 5.13 in water were translucent and rigid regardless of the ring size, whereas in ethanol−water solvents, the degree of opacity varied depending on the cyclic ether. TMO addition resulted in a white, translucent gel in EW (1:1) solution and a white, opaque gel in EW (5:1), whereas PO addition to both EW (1:1) and EW (5:1) solutions produced white, opaque gels. Qualitatively, the opaque gels were less rigid than the translucent gels and were slightly grainy.

Opaque gels formed for reactions with rapid gelation times (5 to 25 s). These relatively fast t_{gel} values are attributed to a combination of solvent and the reactivity of the cyclic ether. Ethanol dramatically increases the rate of reaction, which

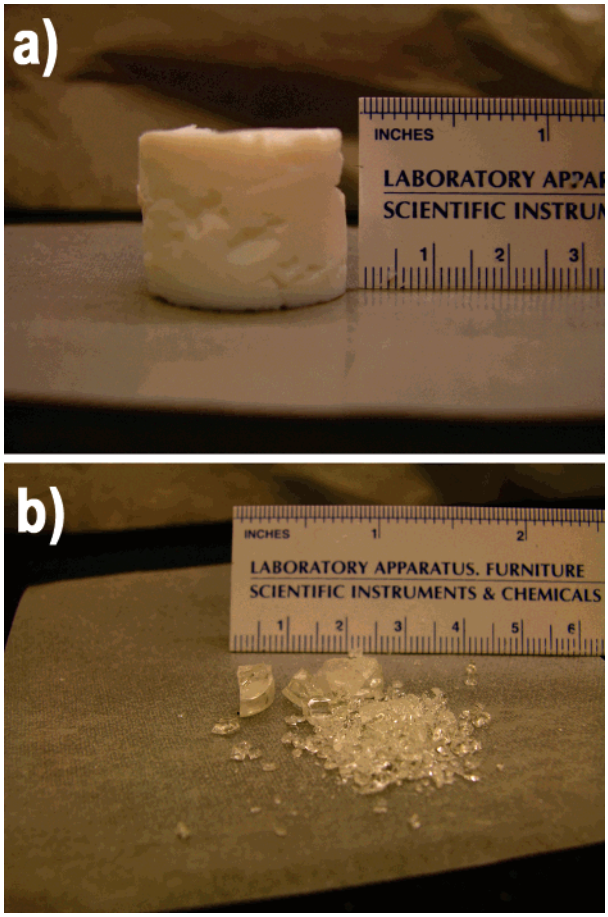

Figure 1. Photographs of (a) as-prepared YSZ aerogel (R_{epox} = 7, R_{H_2O} = 96, and Zr/Y = 2.39) and (b) as-prepared xerogel (R_{epox} = 9, R_{H_2O} = 95, and Zr/Y = 5.13).

may be a result of the improved nucleophilicity of the counterion (Cl^-) in ethanol versus water, resulting in a more rapid opening of the protonated ring. Baumann et al. found similar increased reaction rates for the epoxide-initiated gelation of $AlCl_3 \cdot 6H_2O$ in ethanol versus water and attributed it to this reasoning.[11] It is also possible that decreased solubility of the sol particles occurs in ethanol, leading to rapid condensation of the formed oligomers to give solid gel networks.

Aerogel and Xerogel Processing the YSZ Gels. The gels were very sensitive to the drying step and resulted in significantly different morphologies depending on the drying method. Supercritical drying (aerogels) produced fluffy, soft materials that were easy to grind to an extremely fine powder. Drying under ambient conditions (xerogels), however, resulted in very coarse materials that were difficult to grind beyond a sandlike consistency. Panels a and b of Figure 1 show photographs of typical YSZ aerogel and xerogel materials produced with the epoxide addition method using PO in water. The aerogel was prepared with R_{epox} = 7, R_{H_2O} = 96, and a Zr/Y ratio of 2.39; the xerogel was prepared with R_{epox} = 9, R_{H_2O} = 95, and a Zr/Y ratio of 5.13, where R_{epox} is the molar ratio of epoxide to total metals and R_{H_2O} is the molar ratio of water to total metals. The aerogel shown

(9) Dobinson, B.; Hofmann, W.; Stark, B. P. *The Determination of Epoxide Groups;* Permagon Press: Oxford, U.K., 1969.
(10) Wallace, J. M.; Stroud, R. M.; Pietron, J. J.; Long, J. W.; Rolison, D. R. *J. Non-Cryst. Solids* **2004**, *350*, 31−38.
(11) Baumann, T. F.; Gash, A. E.; Chinn, S. C.; Sawvel, A. M.; Maxwell, R. S.; Satcher, J. H. *Chem. Mater.* **2005**, *17* (2), 395−401.

Table 2. Summary of N_2 Adsorption−Desorption Results as a Function of Reaction Condition for As-Prepared Aerogels[a]

cyclic ether	R_{epox}	R_{H_2O}	SA BET (m^2/g)	pore volume (mL/g)	average pore size (nm)
PO (aerogel)	9	95	453	2.20	15.9
PO (aerogel)	9	EW (1:1)	316	1.74	19.1
TMO (aerogel)	9	95	295	0.646	7.86
TMO (aerogel)	9	EW (1:1)	272	1.32	18.6
TMO (aerogel)	9	EW (5:1)	228	1.16	18.4
TMO (aerogel 550 °C)	9	EW (1:1)	113		
PO (aerogel 550 °C)	7	93	126		

[a] R_{epox} is the molar ratio of cyclic ether to total metals and R_{H_20} is the molar ratio of water to total metals. For the mixed ethanol−water systems (EW (1:1) and (5:1)), R_{H_20} was 95.

in Figure 1a is monolithic; however, care was required to prevent cracks in the wet gels, which results in breaking of the monoliths during the aerogel drying process. The xerogels, however, always cracked and broke apart during drying, preventing the preparation of monoliths.

BET/BJH Surface Area Analysis. Table 2 summarizes the N_2 adsorption−desorption results for several as-prepared aerogels synthesized with a Zr/Y ratio of 5.13. Aerogels that were prepared with PO had larger surface areas than those prepared with TMO. For example, in aqueous solution with $R_{epox} = 9$, the BET specific surface areas for aerogels made with PO and TMO addition were 453 and 295 m^2/g, respectively. The solvent was also an important factor affecting the gel structure. For PO and TMO, the aerogel surface areas were observed to decrease with an increasing ethanol-to-water ratio. For TMO addition in water, EW (1:1), and EW (5:1), the aerogel surface areas were 295, 272, and 228 m^2/g, respectively. For PO addition to water, the surface area was 453 m^2/g, compared with 316 m^2/g in EW (1:1). Unlike the results for varying cyclic ether, here, the surface areas decreased with the shorter t_{gel} times of the ethanol solutions. The shorter t_{gel} is attributed to the greater nucleophilicity of the chloride anion in ethanol, and the smaller surface area is attributed to destabilizing of the sols in ethanol, resulting in greater colloid growth. This is supported by the formation of opaque, grainy gels at higher ratios of ethanol to water. The opaque gel formed with TMO addition in EW (5:1) did not have a considerably lower surface area than the translucent gels that were formed in water and in EW (1:1), suggesting that the morphology is similar but possibly contains larger particulate sizes. This is confirmed with TEM data, which will be presented later.

The PO-derived aerogels had larger pore volumes than similarly prepared TMO derived aerogels; however, a trend as a function of solvent was not apparent (see Table 2). In aqueous solutions with PO and TMO addition, the pore volumes were 2.20 and 0.646 mL/g, respectively, and in EW (1:1), they were 1.74 and 1.32 mL/g. Increasing the ethanol to 5:1 with TMO addition resulted in a decrease in pore volume to 1.16 mL/g. The average pore size was nearly identical for the ethanol−water-derived aerogels regardless of cyclic ether and was observed to decrease for samples prepared in water. The pore sizes ranged from 8 to 20 nm, indicating the materials are mesoporous in nature.

The shape of the adsorption−desorption isotherms depended upon the solvent and drying step but not upon the choice of cyclic ether initiator. Panels a and b of Figure 2 show typical isotherms for aerogels prepared with TMO in water and EW (1:1), respectively. Aerogels prepared with

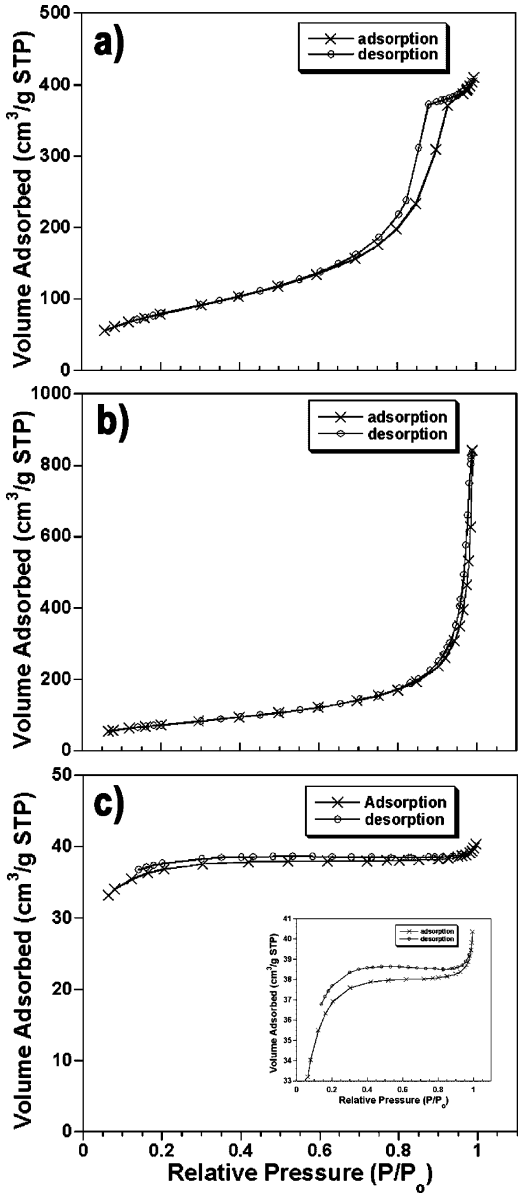

Figure 2. Nitrogen adsorption−desorption isotherms for gels prepared with $R_{epox} = 9$ and Zr/Y = 5.13: (a) as-prepared aerogel (TMO in water), (b) as-prepared aerogel (TMO in EW (1:1)), and (c) as-prepared xerogel (PO in water). The insert in c shows a reduced axis to demonstrate the sigmoidal shape of the isotherm.

PO showed similar isotherms for a given solvent. The aerogel prepared in water (Figure 2a) had a Type IV isotherm with a plateau at high relative pressure and a closed desorption branch hysteresis loop.[12] The aerogel prepared in ethanol−water (Figure 2b) also displayed a Type IV isotherm, but without the plateau and less hysteresis. The majority of

adsorption occurring at high relative pressures and the presence of closed hysteresis loops suggests that the aerogels are primarily mesoporous materials (pore diameters = 2−50 nm).[12] The physisorption process occurs in two steps, monolayer−multilayer adsorption and capillary condensation within the pores.[12] The monolayer−multilayer adsorption−desorption, occurring at low relative pressures, is the same regardless of solvent or cyclic ether. The difference due to solvent occurs at higher relative pressures and is related to the condensation in mesopores, indicating that the solvent affects the nanostructure of the aerogel networks.

Xerogel-processed gels were different from those processed as aerogels. Figure 2c shows the adsorption−desorption isotherm for a PO-derived xerogel prepared in water. The xerogel had a Type II isotherm, showing the typical sigmoidal shape in the adsorption branch.[12] Compared with the aerogel materials, the volume adsorbed was significantly lower, indicating the absence of large pore volume. Most of the adsorption process occurred at low relative pressure, signifying both monolayer−multilayer adsorption and micropore filling. Also, the desorption branch displayed an open hysteresis loop extending to the lowest attainable pressure, further suggesting the presence of micropores associated with irreversible uptake of molecules in the pores.[12] The Type II isotherm is typical of materials that are either microporous or nonporous, consistent with the coarse nature of the xerogel products. SEM analysis, which further confirms the low pore volume and lack of mesopores in the xerogel, will be discussed later.

BET analyses of adsorption isotherms for xerogels prepared with PO or TMO in water were attempted; however, large negative values for C_{BET} were obtained.[13] C_{BET}, from the BET equation, is related to the enthalpy of adsorption; negative values have no physical meaning, indicating that BET calculations are not reliable for these materials. This problem is associated with the fact that BET calculations do not account for micropore filling, which is observed for the xerogels.[12]

Electron Microscopy of Aerogels and Xerogels. The macroscopic morphology differences between aerogel- and xerogel-processed gels translated to the microscopic scale and were clearly observed with electron microscopy. The as-prepared and calcined aerogels were soft, easy to grind, and for the calcined material, consisted of very homogeneous, discrete nanoparticles. In contrast, the as-prepared and calcined xerogels were coarse, difficult to grind, and composed of heterogeneous micrometer-sized hard agglomerates. Panels a and b of Figure 3 show SEM micrographs for an as-prepared TMO-derived xerogel (R_{epox} = 9, EW (1:1), Zr/Y = 5.13) at different magnifications. The low-magnification image (Figure 3a) gives an example of the micrometer-sized agglomerates found in the material. The agglomerates were heterogeneous in size and shape, ranging from submicrometer to more than 10 μm. The high-magnification image (Figure 3b), revealing the smooth surfaces of the agglomerates and the absence of mesopores, is consistent with nitrogen adsorption−desorption results (Table 2 and Figure 2c); however, the presence of micropores (<2 nm), suggested by the N_2 adsorption−desorption isotherms, is not observable at this magnification.

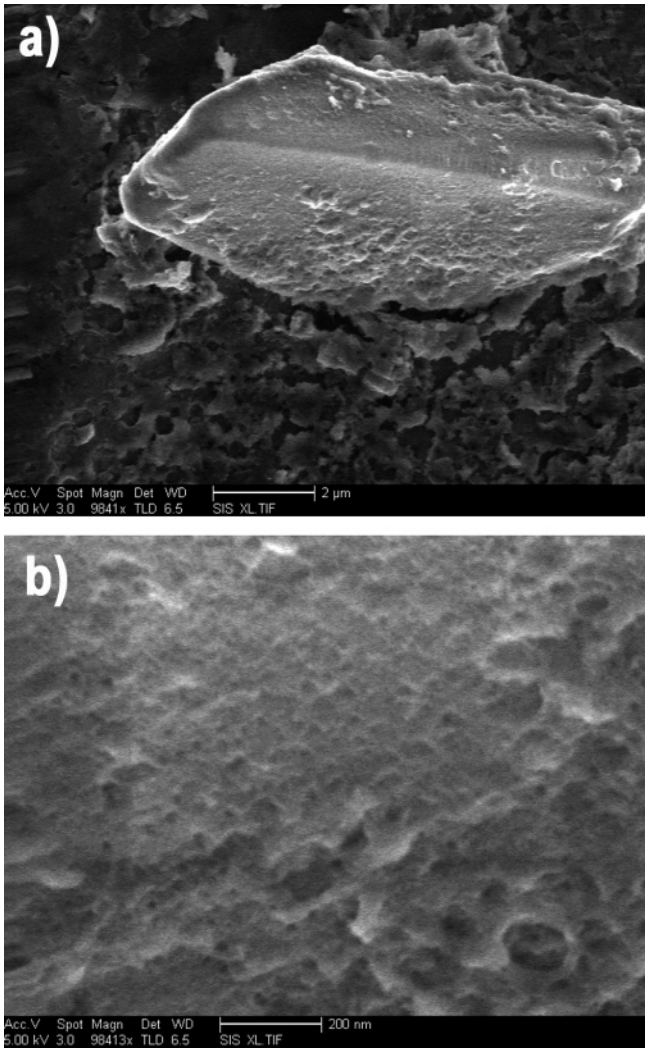

Figure 3. SEM micrographs of an as-prepared YSZ xerogel prepared with TMO (R_{epox} = 9) in EW (1:1) and Zr/Y = 5.13 at (a) low and (b) high magnification.

The aerogel processing, regardless of solvent or cyclic ether, produced amorphous, extended nanoparticulate networks, distinctly different from the dense agglomerates observed in the as-prepared xerogel. The degree of networking and size of the particulates, however, varied depending on solvent and cyclic ether. Brightfield TEM micrographs of the TMO-derived YSZ aerogels prepared in water, EW (1:1), and EW (5:1) are shown in Figure 4a−c, respectively. Aerogels prepared with PO in water and in EW (1:1) are shown in Figure 5a,b. The aerogels shown here are from the samples used in the nitrogen adsorption−desorption studies (Table 2 and Figure 2a,b) and were mesoporous, consistent with the pore size and volume determinations.

The aerogel prepared with TMO in water (Figure 4a) shows less networking and a more densely packed particulate nature than do the aerogels prepared with TMO addition to ethanol−water solutions (Figure 4b,c). The significantly smaller pore volume and average pore size (Table 2)

(12) Sing, K. S. W.; Everett, D. H.; Haul, R. A. W.; Moscou, L.; Pierotti, R. A.; Rouquerol, J.; Siemieniewska, T. *Pure Appl. Chem.* **1985**, *57* (4), 603−619.
(13) Kooli, F.; Kiyozumi, Y.; F., M. *New J. Chem.* **2001**, *25*, 1613−1620.

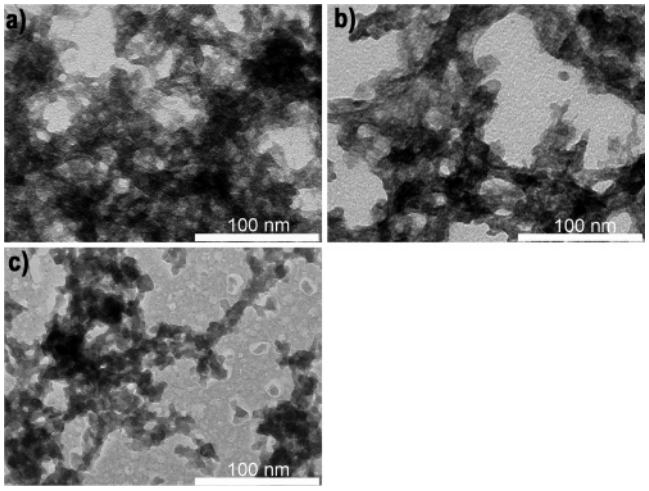

Figure 4. Brightfield TEM micrographs of as-prepared YSZ aerogels prepared with TMO in (a) water (b) EW (1:1) and (c) EW (5:1).

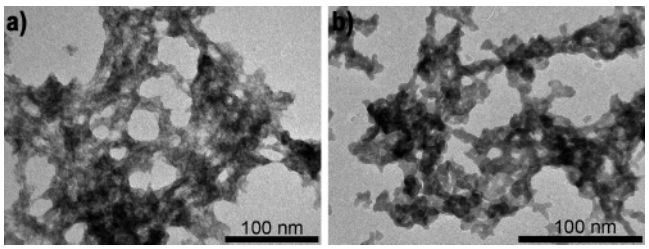

Figure 5. Brightfield TEM micrographs of as-prepared YSZ aerogels prepared with PO in (a) water and (b) EW (1:1).

calculated for the aerogel in Figure 4a is consistent with these results. The aerogel prepared with EW (1:1), however, had similar particulate sizes, which were too small to be resolved. Conversely, the aerogel prepared in EW (5:1) had distinctly larger particulate sizes, consistent with the lower surface area found for this aerogel. The aerogel prepared with PO in water (Figure 5a) also displayed a fine nanostructured network. The nanostructures are presumably formed by olation and oxolation of hydrated Zr(IV) and Y(III) monomers to form oligomers (colloids) that eventually cross-link to give a solid gel network.[2]

The reaction conditions that produced translucent, rigid gels resulted in finer sized particulates in the as-prepared aerogels (Figures 4a, 4b, and 5a), whereas relatively fast reaction conditions that produced opaque, grainy gels resulted in large particulate sizes (Figures 4c and 5b). Networking is observable for the larger particulate gels, and although they were qualitatively less rigid, monoliths were still formed. The microscopy results support the proposal, set earlier, that ethanol increases colloidal growth in solution resulting in larger particulate formation (lower surface areas). Solvent plays a role in the stability of the sol, and ethanol appears to destabilize the colloids, resulting in increased particle growth. This effect occurs at lower ethanol-to-water ratios with the more reactive PO, in which hydrolysis and condensation of the cation species occurs more rapidly.

ICP−AES Analysis. Table 3 summarizes elemental analysis results for YSZ aerogels prepared with PO addition ($R_{epox} = 9$) to aqueous solutions having Zr/Y ratios ranging from 16.2 to 1.67, corresponding to 3.09−25.0 mol % Y_2O_3-stabilized zirconia. The samples were calcined to 1000 °C for 1 h before analyses. The expected and analysis results for the Y_2O_3 content agreed well for samples prepared with 3.09, 9.09, and 17.7 mol % Y_2O_3, whereas the determined Y_2O_3 content for the sample prepared with 25 mol % was lower than expected (23%). The chloride and carbon content of the calcined aerogels, also listed in Table 3, were below 20 ppm and 0.5 wt %, respectively. The different reaction rates of the cations becomes evident for a Zr/Y ratio of 1.67 (25.0 mol % Y_2O_3-stabilized zirconia), in which a lower than expected Y_2O_3 substitution is observed. Greater incorporation of Y_2O_3 may be achievable by increasing R_{epox}, thereby increasing the rate of gelation, or by starting with a larger concentration of $YCl_3 \cdot 6H_2O$ in the precursor solution.

Table 3. Elemental Analysis Results for Various Ratios of Zr/Y

R_{epox}	R_{H_2O}	expected Zr/Y	analysis Zr/Y	expected mol %	analysis mol %	Cl %	C %
6	92	16.1	16.2	3.09	3.07	0.04	0.05
7	93	5.13	5.11	9.09	8.91	n.d.[a]	<0.5
7	96	2.39	2.44	17.7	17.0	<19 ppm	
7	96	1.54	1.67	25.0	23.0	<21 ppm	

[a] n.d. = not determined.

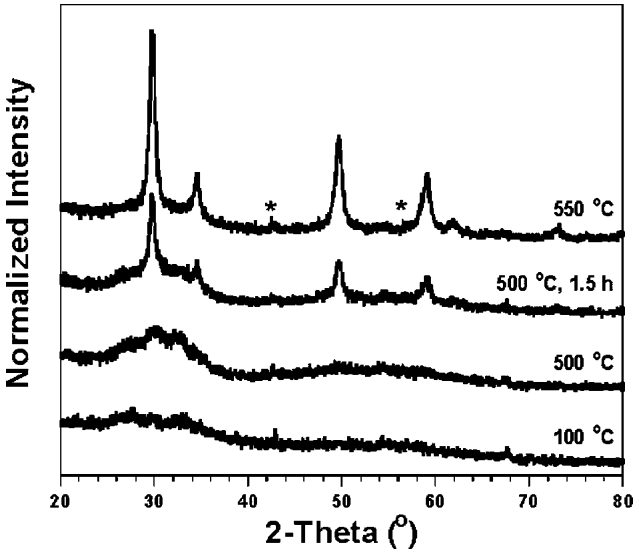

Figure 6. In situ temperature profile XRD of a YSZ aerogel prepared with TMO in EW (1:1). Diffraction patterns were measured immediately after reaching each temperature and once again after dwelling for 1.5 h. Only selected diffraction profiles are shown to prevent redundancy. Additional peaks associated with the Al_2O_3 sample holder become apparent during shrinkage of the sample during heating. The sharp Al_2O_3 peaks are easily distinguished from the broad (nanocrystalline) YSZ phase and are marked with an asterisk (*).

Powder X-ray Diffraction. The in situ powder X-ray diffraction results for a YSZ aerogel prepared with TMO ($R_{epox} = 9$) in EW (1:1) are shown in Figure 6. The as-prepared aerogel was X-ray amorphous and remained so up to 500 °C. Prolonged calcination at 500 °C for 1.5 h, however, resulted in crystallization of stabilized zirconia. This result is different than the previously reported result for YSZ prepared with PO in water, in which the aerogel was partially crystalline upon reaching 500 °C and became more crystalline with prolonged heating at that temperature.[2] The reason for this difference in crystallization temperature

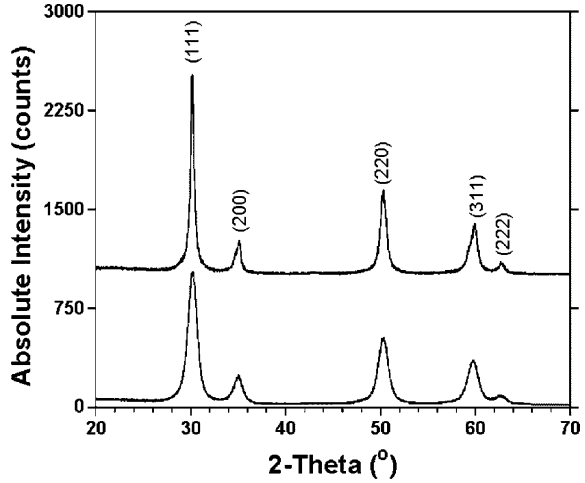

Figure 7. Powder XRD patterns for an aerogel and xerogel prepared with TMO in EW (1:1) and calcined at 550 °C: YSZ aerogel (bottom) and xerogel (top).

is not known but may be related to the greater reactivity of the higher surface area particles prepared with PO addition.

The in situ results demonstrate that crystalline material can be prepared at 500 °C; however, for further XRD and TEM analysis, calcination at 550 °C was chosen to ensure crystallinity in the products. Figure 7 shows the XRD patterns for aerogel- and xerogel-processed gels prepared with TMO in EW (1:1) and a Zr/Y ratio of 5.13. Both samples formed single-phase stabilized zirconia and were nanocrystalline, as is evident by peak broadening. The average crystallite sizes, calculated from the Scherrer formula, were 33 and 9.4 nm for the xerogel and aerogel, respectively. In general, xerogels are denser compared with their aerogel counterparts because pore walls collapse under capillary forces created by the evaporating solvent. The densification of the gel structure results in larger average crystallite size upon calcining.

The diffraction pattern for a calcined aerogel prepared with PO in water (provided in the Supporting Information) was similar to those shown in Figure 7 but had slightly greater peak broadening. The average crystallite size, calculated from peak broadening of the PO-derived sample was 6.0 nm, compared with 9.4 nm for the TMO-derived YSZ shown in Figure 7. The average particle sizes (d_{BET}) for the two samples were calculated from the experimentally determined BET specific surface areas (Table 2) as described previously.[2] For the PO and TMO samples, the BET specific surfaces areas were 126 and 113 m^2/g, corresponding to d_{BET} of 8.0 and 8.9 nm, respectively. The average crystallite size and particle size show good agreement, indicating that the primary particles of the calcined powder are single crystals. This is further supported by TEM data.

Structural Analysis of Calcined Aerogels. Room-temperature XRD patterns for samples calcined to 1000 °C and analyzed with ICP−AES (Table 3), corresponding to 3.07, 8.91, and 17.0 mol % Y_2O_3-stabilized zirconia, were measured. The calcined aerogel, corresponding to 3.07 mol % YSZ, is shown in Figure 8a. Both tetragonal (PDF# 62-9436) and monoclinic (PDF# 64-9594) phases are observed, consistent with reported mixed-phase monoclinic−tetragonal,

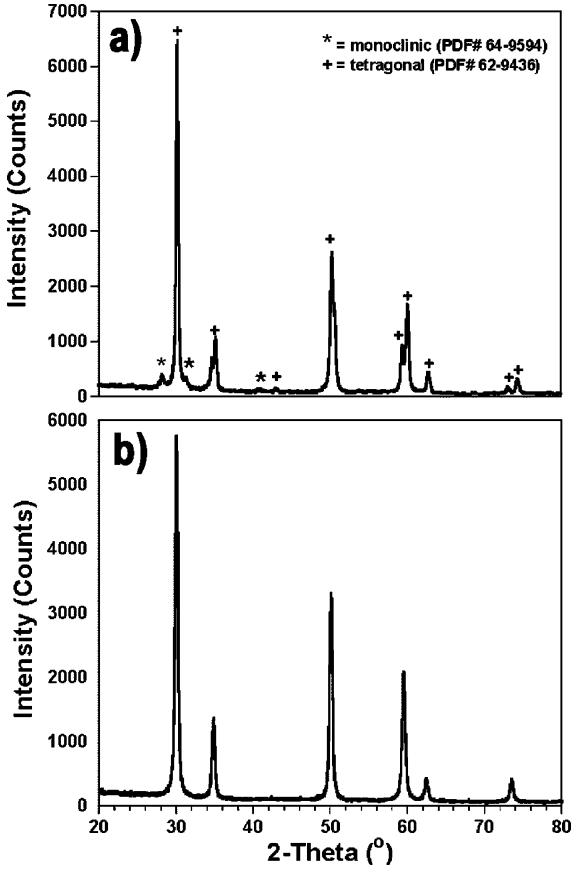

Figure 8. Powder XRD patterns for calcined YSZ (1000 °C): (a) aerogel prepared with PO ($R_{epox} = 9$) in water and Zr/Y ratios corresponding to 3.07 mol % Y_2O_3 and (b) commercial YSZ (Tosoh TZ-8Y) reported as 7.69 mol % YSZ.

partially stabilized zirconia at that composition.[14] XRD patterns for the 8.91 and 17.0 mol % YSZ samples were single-phase stabilized zirconia, with diffraction patterns similar to those presented in Figure 7. The peaks were narrower, however, because of the larger crystallite sizes resulting from the higher calcination temperature. For comparison, a commercial YSZ powder prepared by hydrolysis (Tosoh TZ-8Y, Japan) and reported by the manufacturer to be 7.69 mol % YSZ, is shown in Figure 8b and displays peaks similar to the 8.91 and 17.0 mol % YSZ. These three patterns could be indexed as either cubic (PDF# 82-1246) or tetragonal (PDF# 82-1245) zirconia.

It is known that the relatively small atomic scattering factor of oxygen makes it difficult to distinguish with XRD between the cubic and tetragonal phases of YSZ near the phase boundary (8−10 mol % Y_2O_3).[15] This difficulty is compounded for nanocrystalline materials, because of peak overlap due to broadening effects. The cubic-to-tetragonal phase transition in doped zirconia occurs by both elongation of one of the crystallographic axes relative to the other two[16] and displacement of oxygen from the ideal anion site in the fluorite structure.[17] Raman spectroscopy, which is sensitive

(14) Sato, T.; Shimada, M. *J. Mater. Sci.* **1985**, *20* (11), 3988−3992.
(15) Yashima, M.; Sasaki, S.; Kakihana, M.; Yamaguchi, Y.; Arashi, H.; Yoshimura, M. *Acta Crystallogr., Sect. B* **1994**, *50*, 663−672.
(16) LeFevre, J.; Collongues, R.; Jorba, M. P. Y. *C. R. Acad. Sci.* **1959**, *249*, 2329−2331.
(17) Teufer, G. *Acta Crystallogr.* **1962**, *15*, 1187.

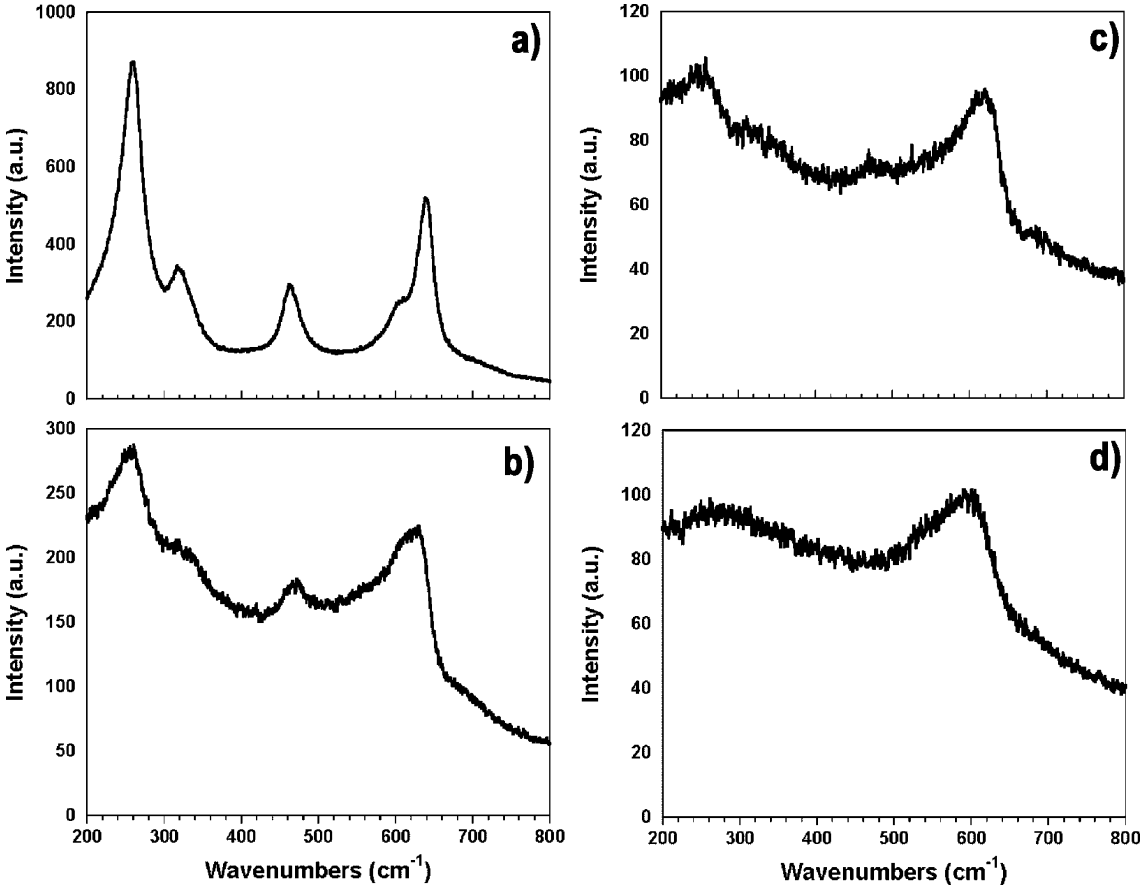

Figure 9. Raman spectra for calcined YSZ powders with Zr/Y ratios corresponding to Y_2O_3 mol % of (a) 3.07, (b) 7.69 (Tosoh TZ-8Y), (c) 8.91, and (d) 17.0.

to polarizability of the oxygen ions and provides information on local structure not observed in powder XRD, can be used to clarify the structure.[18]

Raman Spectroscopy. Raman spectra for YSZ with increasing mol % of Y_2O_3 and calcined at 1000 °C are shown in Figure 9a−d. The spectra are for samples characterized with XRD (Figure 8) and elemental analysis (Table 3) and clearly demonstrate the transition from tetragonal to cubic phase with increasing Y_2O_3 substitution. The Raman spectrum for the tetragonal phase is characterized by six relatively sharp peaks at approximately 115, 266, 326, 474, 616, and 646 cm^{-1}.[18] The spectrum for the cubic phase, however, is characterized by a single broad peak in the range of 530−670 cm^{-1} and additional poorly defined structures related to the disordered oxygen sublattice.[19, 20]

The Raman spectrum for 3.07 mol % YSZ, shown in Figure 9a, displays peaks associated with the tetragonal phase. However, the XRD pattern (Figure 8a) for this sample indicated that a small amount of monoclinic phase is present along with the predominant tetragonal phase. The monoclinic phase was not observed in the Raman spectrum, possibly because of the overlap with the broad and relatively intense tetragonal peaks. The 7.69 mol % commercial YSZ (Tosoh TZ-8Y), shown in Figure 9b, displayed some tetragonal characteristic with peaks at 258 and 468 cm^{-1} and a broad shoulder at 325 cm^{-1}. Additionally, a broad peak from 588 to 640 cm^{-1}, associated with the cubic phase, is observed. These results are consistent with reported mixed phase tetragonal-cubic, partially stabilized zirconia below 9 mol % Y_2O_3.[21] The 9.49 mol % YSZ, shown in Figure 9c, was predominantly cubic with a broad peak from 578 to 635 cm^{-1} and had significantly less tetragonal characteristic than did the 7.69 mol % YSZ. However, there were still broad, poorly defined peaks at 253 and 478 cm^{-1}, corresponding to the tetragonal phase. In Figure 9d, a sample with 17.0 mol % Y_2O_3 is shown. Only a broad peak from 508 to 625 cm^{-1}, associated with the cubic structure, is observed in this sample.

Comparing the XRD patterns with the corresponding Raman spectra is an excellent way to determine the phases present in yttria-stabilized zirconia, particularly around the tetragonal−cubic phase boundary, where XRD may not be sufficient. In this study, Raman spectroscopy was useful in demonstrating that 7.69 (commercial, hydrolysis) and 9.49 (aerogel derived) mol % YSZ contain a detectable amount of tetragonal character, whereas XRD analysis was ambiguous. Possibly, part of the difficulty is related to the abundance of the tetragonal phase, which may be below the detection limits of XRD (~5 wt %), yet observable with the very sensitive Raman experiments. These results are of interest to the fuel cell community because often 8 mol % YSZ is referred

(18) Feinberg, A.; Perry, C. H. *J. Phys. Chem. Solids* **1981**, *42* (6), 513−518.
(19) Keramidas, V. G.; White, W. B. *J. Phys. Chem. Solids* **1973**, *34*, 1873.
(20) Kontoyannis, C. G.; Orkoula, M. *J. Mater. Sci.* **1994**, *29* (20), 5316−5320.
(21) Yashima, M.; Ohtake, K.; Kakihana, M.; Arashi, H.; Yoshimura, M. *J. Phys. Chem. Solids* **1996**, *57* (1), 17−24.

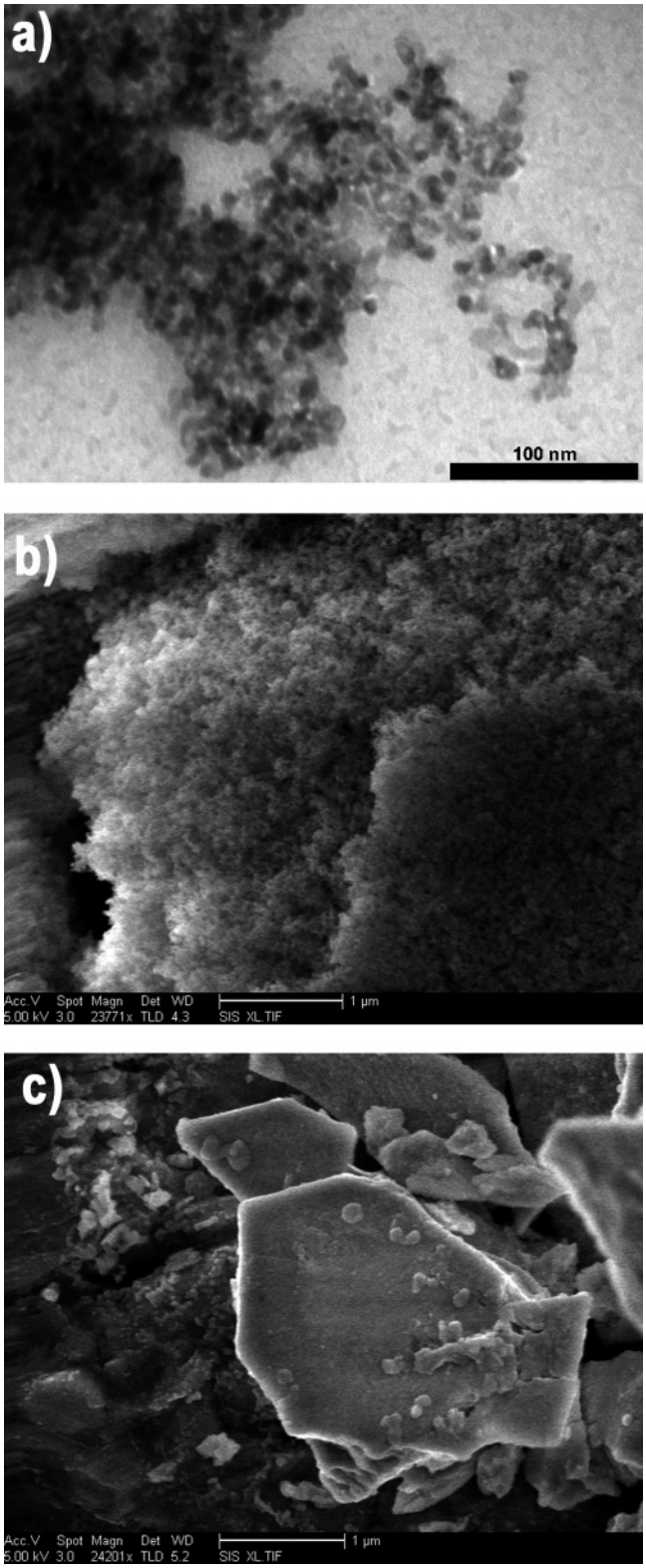

Figure 10. Micrographs of an aerogel and xerogel prepared with TMO in EW (1:1) and calcined at 550 °C: (a) brightfield TEM micrograph of the aerogel, (b) SEM micrograph of the aerogel, and (c) SEM micrograph of the xerogel.

to as cubic-stabilized zirconia based on XRD data alone. However, as observed here for samples prepared by different methods (epoxide addition method and hydrolysis) there is still some tetragonal character present. The cubic structure at the lower stabilization limit is known to have the highest ionic conductivity and therefore optimizing synthetic and powder treatment to maximize conductivity should include a combination of Raman and XRD characterization.[1]

Electron Microscopy of Calcined Aerogels and Xerogels. Calcination of the aerogels to 550 °C produced crystalline YSZ composed of discrete spherical nanoparticles, which aggregated but did not form hard agglomerates. Figure 10a shows a TEM micrograph of the aerogel prepared with TMO addition to a EW (1:1) solution and calcined to 550 °C. The image provides resolution of the individual particles, demonstrating their size and morphology. The particles have diameters less than 10 nm, and the extended network of the original aerogel is no longer present. The TEM results agree well with the average crystallite size (9.4 nm) and particle size (8.9 nm) determined from XRD and BET analysis. In Figure 10b, an SEM micrograph of the same calcined aerogel is shown to demonstrate the homogeneous nature of the YSZ, the absence of hard agglomeration, and the presence of aggregation common to high-surface-area oxide nanoparticles. This example is typical for calcined YSZ aerogels. The as-prepared powder morphologies, which varied with cyclic ether and solvent, are not retained with calcination as the networks decompose along with significant weight loss (∼30%) to form the spherical nanoparticles.

The calcined xerogels had distinctly different morphologies than did the aerogels. The powders consisted of a heterogeneous distribution of micrometer-sized hard agglomerates, which had morphologies similar to those of the as-prepared xerogel precursors (Figure 4a,b). The SEM micrograph, shown in Figure 10c, highlights this result. The agglomerates observed in the calcined xerogel consists of primary crystallite sizes on the nanometer scale, as observed with peak broadening in the XRD pattern (Figure 6). These agglomerates, however, are extremely strong and do not break apart to nanometric dimensions with standard milling techniques.

Conclusions

Powder morphology is critical for applications involving YSZ, and particle size and size distribution are important factors to be considered when fabricating devices.[22,23] Homogeneous powders consisting of submicrometer particles, free of hard agglomeration, can be beneficial for many fabrication techniques, including slip casting, tape casting, isostatic pressing, and colloidal spray deposition.[24,25] Additionally, nanoparticles can potentially benefit ceramic processing by lowering sintering temperatures, increasing firing density, and creating nanosized grains in the fired ceramics on the basis of their large surface energies.[24,26,27] YSZ aerogels prepared through the epoxide addition method have remarkably high surface areas and nanoparticulate

(22) Sasaki, K.; Wurth, J. P.; Gschwend, R.; Godickemeier, M.; Gauckler, L. J. *J. Electrochem. Soc.* **1996**, *143* (2), 530−543.
(23) Kim, J. D.; Kim, G. D.; Moon, J. W.; Lee, H. W.; Lee, K. T.; Kim, C. E. *Solid State Ionics* **2000**, *133* (1−2), 67−77.
(24) Mistler, R. E.; Twiname, E. R. *Tape Casting: Theory and Practice*; Amercian Ceramic Society: Westerville, OH, 2000.
(25) Xu, G.; Zhang, Y.-W.; Liao, C.-S.; Yan, C.-H. *Solid State Ionics* **2004**, *166* (3−4), 391−396.
(26) King, A. G. *Ceramic Technology and Processing;* William Andrew Publishing: New York, 2002.
(27) McColm, I. J. In *Ceramic Processing*; Terpstra, R. A., Pex, P., De Vries, A., Eds.; Chapman and Hall: New York, 1995; pp 17−18.

morphologies even after calcination at 550 °C, and thus may be exciting new nanomaterials for ionic conducting devices, whereas the xerogels, because of the dramatic densification of the gels during the ambient drying process, are far too coarse for most ceramic applications.

The cyclic ether and solvent were found to be critical factors in the resulting as-prepared aerogel surface area and morphology. Aerogels prepared with the epoxide (PO) had higher surface areas than did those prepared with the oxetane (TMO) for a given solvent. Aerogel surface areas also decrease with increasing ethanol in the solvent. This is attributed to instability of the sol in ethanol, resulting in rapid condensation and colloid growth. This effect, which results in larger particulate formation, occurs at lower ethanol-to-water ratios with the more reactive epoxide, in which hydrolysis and condensation of the cation species occurs more rapidly. The crystallized YSZ, however, displayed similar morphologies regardless of the solvent and cyclic ether effects. The various as-prepared aerogel morphologies decompose with calcination to 550 °C to produce homogeneous, nanocrystalline powders.

The combined elemental analysis, electron microscopy, and XRD results suggest that Y^{3+} incorporates homogeneously within the Zr^{4+} nanostructure during gelation over a wide range of Y^{3+} substitution. The actual reaction rates may vary for the two cations, but the rapid gelation conditions (PO in water) do not appear to lead to segregation of the cations in the gel or pore solvent. Microscopy data demonstrates the homogeneous nature of the aerogel material before and after calcination and XRD analysis shows an absence of intermediate oxide formation before crystallization of stabilized zirconia. Additionally, the low temperature of crystallization suggests that significant mass diffusion is not required to form YSZ.

Acknowledgment. This work was supported by the University of California Energy Institute, the National Science Foundation (Grant DMR-0120990, -0600742), and the Department of Energy (Student Employee Graduate Research Fellowship). The authors thank Julie Muyco for Raman spectroscopy measurements, Alexandra Navrotsky for use of the Scintag diffractometer, and David W. Sprehn for technical support. This work was performed under the auspices of the U.S. Department of Energy by the University of California, Lawrence Livermore National Laboratory, under Contract W-7405-Eng-48.

Supporting Information Available: Powder XRD patterns for YSZ aerogels calcined at 550 °C prepared with TMO in EW (1:1) and PO in water (pdf). This material is available free of charge via the Internet at http://pubs.acs.org.

CM061258C